Digest Journal of Nanomaterials and Biostructures Vol. 17, No. 4, October-December 2022, p. 1463-1474

Physical properties of thin films of (α-Fe_2O_3) aluminum doped by spray pyrolysis methods

A . Chibani[a,*], D. Kendil[b] , B . Benhaoua[c], I. Kemerchou[d], D. Bekkar[e]
[a]*Laboratory of Coatings, Materials and Environment, UMBB, Boumerdes-University, , 35000, Algeria*
[b]*Sensor-based integrated systems laboratory((LSIC), Higher Normal School - Ecole Normale Supérieure - ENS– Kouba16000 , ALGERIA*
[c]*Lab. VTRS, Faculty of Technology, Univ. El-Oued, El oued 39000, Algeria*
[d]*Department of Electrical Engineering, Faculty of Applied Science, University of Ouargla, 30000, Algeria*
[e]*Faculty of Exact Sciences, Univ. El-Oued, El oued 39000, Algeria*

This work aims to study the effect of doping on α-Fe_2O_3 properties. For this, we elaborated thin layers of pure α-Fe_2O_3, and aluminum doped with spray pyrolysis method. The structural, morphological, and optical properties of the prepared films form different percentages: 2%, 4%, 6%, 8%and 10% were examined using X-ray diffraction (XRD), FT-IR, and UV-Vis, respectively. Structural characterization from X-ray diffractograms confirmed the formation of α-Fe_2O_3, it has a rhombohedral structure with strong orientation preferential according to a plane (110) and displacement of the diffraction angles towards large values when the doping rate increases. Studies of transmittance spectra in UV-visible range 550-850 nm, showed high transparency of thin layers elaborated and the increase in direct band-gap energy from 2.59 to 2.78 eV. These characteristics are considered important in all applications.

(Received September 13, 2022; Accepted December 14, 2022)

Keywords: Thin layers, α-Fe_2O_3, Pyrolysis spray, FT-IR; XRD

1. Introduction

Metal oxides belonging to family of transparent and conductive oxides (TCO) are remarkable materials and have applications in many fields[1]. The metal, we have chosen is iron and we will study the properties of their oxides by carrying out their optical characterizations to evaluate their performance in photocatalysis. For this, we will prepare a series of thin layers of iron oxide by varying different doping percentages. The spray pyrolysis method has the advantages of being simple, easy, and quick[2][3]. We are interested in the study of optical characteristics using different technical characterizations.

Iron is found in nature in the form of molecular complexes, colloids, oxides, oxyhydroxides, and hydroxides. In addition, the iron atom is also present in biological components such as hemoglobin. It is widely used in various fields such as metallurgy, colored pigments, magnetic materials, catalysts, etc.[4] [5].

Iron in the solid phase (mostly iron(III)) is essentially bound to oxygen to form hydroxides, oxyhydroxides, and oxides of iron which play a very important role.

Iron oxides are widespread in nature and can be easily synthesized in laboratories. They are found in the earth's crust (rock, ore), in water (water erosion, rivers...) and in biological organisms (human body, animals, plants). They were used very early by man: already, in prehistoric times, cave paintings contained iron oxide pigments. Then, they were used in many other fields (physics-chemistry-biology)[6]. They have interest for applications in many scientific and industrial fields, environmental applications, corrosion, soil science and biology, etc. [7].

* Corresponding authors: ab.chibani@univ-boumerdes.dz
https://doi.org/10.15251/DJNB.2022.174.1463

Pigments containing iron oxide are used in coatings and as colorants in ceramics, glass, plastics, and rubber. In nature, there are approximately seventeen (16) known iron oxides, hydroxides, and oxyhydroxides which represent more than 5% of the weight of the earth's crust. All consist of Fe, O, and/or OH atoms that differ in composition, in the valence of Fe, and especially in the structure of the crystal. Iron oxides, iron hydroxides, and iron oxyhydroxides are distinguished by the different Greek letters:α, β, et γ which symbolize the different polymorphs [8][9]. There are several ways to classify these compounds: according to the iron oxidation number (divalent, trivalent, or mixed divalent-trivalent iron), according to the chemical formula (oxide, hydroxide) and finally according to the two-dimensional or three-dimensional nature of the crystal structure.

The development of materials in thin layers is of major interest, in very varied application fields. Development of new technological solutions requires depth knowledge of different materials categories, their structure, their properties, and the slightest knowledge of their manufacturing processes. In recent years, iron oxides are the most important transition metal oxides. They are best known and most studied magnetic materials, as they occur in nature and are easy to synthesize. In general, preparation conditions of thin layers α-Fe_2O_3 by spray pyrolyse process have a major influence on the properties of these layers [10]. It is, therefore, necessary to systematically study the physical properties (structural, optical, etc.) of thin films of α-Fe_2O_3.

To contribute to a better understanding of the effect of the thin layer on the physical properties of the semiconductor, we undertook the present work which consists in developing thin layers of pure and aluminum-doped α-Fe_2O_3 and carrying out a study of their properties, in order to study and optimize the levels of doping which makes it possible to have high transmittance. This work includes description of the experimental methods which allowed the elaboration and the characterization of the α-Fe_2O_3 semiconductor samples elaborated, as well as the discussion of the results concerning the structural, and optical characterizations of the thin layers of pure and α-Fe_2O_3 doped Aluminum. The most well-known metal oxides are iron oxides and hydroxides. Iron compounds are abundant in nature and have a wide range of scientific applications, including catalysts[11], soil treatment[12][13], and antibacterial applications in medicine[14][15]. Iron oxides are appropriate for use as paints and pigments due to their stability and lack of toxicity[16][17]. Sand covered with iron oxide has previously been demonstrated to have high effectiveness in eliminating a variety of pollutants from water/wastewater[18][19]. Black iron oxide (Fe_3O_4), magmite (γ -Fe_2O_3), and hematite (α -Fe_2O_3) are the three most frequent iron oxides in nature that are very essential technologically[20]. Due to their small size, huge surface area, and magnetic characteristics, iron oxide nanoparticles (NPs) have recently gained increased interest in environmental cleanup [21].

2. Materials and methods

2.1.Thin films preparation

The aluminum-doped iron oxide was prepared using the thermochemical spray deposition method ¸to obtain a mother solution of 0.25M of Fe_2O_3 dissolved in 2.027g of iron chloride ($FeCl_3$) in 50 mL of distilled water and ethanol.

It is well mixed at room temperature with a magnetic mixer until complete dissolution (red-brown solution).

Different from aluminum Al to this solution while continuing to stir for an hour to obtain a set of concentrations of the grafts (2, 4, 6, 8, and 10).

The obtained mixtures were sprayed on glass substrates heated at 500 °C with dimensions (3.75 x 2.5 x 0.13) Sedimentation process was at a rate of 10 times back and forth at a spray rate of 5 ml / min cm^3, substrate is 5 cm distance from moving nozzle

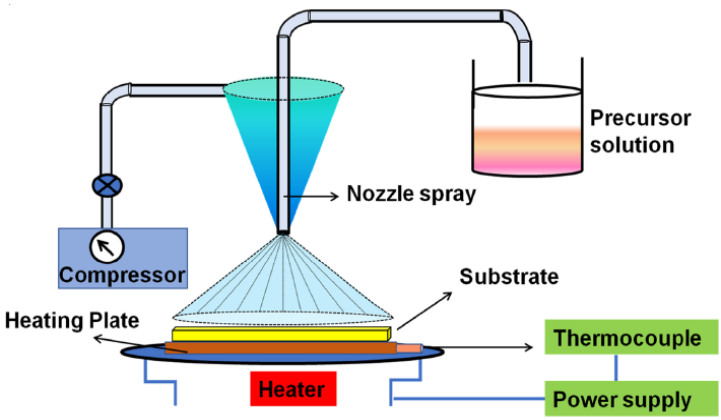

Fig. 1. Spray pyrolysis technique with moving nozzle (SPMN).

2.2. Thin films characterization

The crystallographic structure of 0-10 wt % Al-doped α-Fe_2O_3 thin films have been examined via a Philips X-ray diffractometer model PW-1710. Optical properties such as transmittance and band gaps have been undergone Using a (UV–VIS spectrophotometer Shimadzu, Model 1800) that works in the 300–900nm wavelength range, we looked at the optical transmittance spectrum.. Whereas FT-IR analysis was performed, in 400- 4000cm^{-1} range, by use of Shimadzu IR-Infinity 1 apparatus. All the measurements were carried out at room temperature.

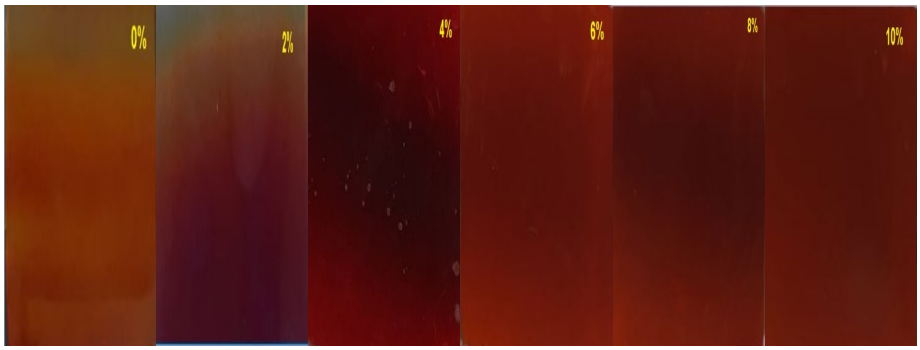

Fig 2. Photographs of elaborated samples of 0-10% wt Al-doped α-Fe_2O_3 thin films.

3. Results and discussions

After Al doping, with different percentages, we can view that some components come, and others leave. So, technical and chemical characterization of thin film results, are different for initial no doped

3.1. Structural characterization of α-Fe_2O_3

3.1.1. X-ray diffraction

Using the copper anticathode X-ray source (λ= 1.5406 Å). The X-ray diagram of an α-Fe_2O_3 thin film according to JCPDS (JCPDS No: 01.073- 2234) is shown in Figure3. From the data of this diffractogram specific to α-Fe_2O_3, which we used to identify the different diffraction peaks measured on our samples

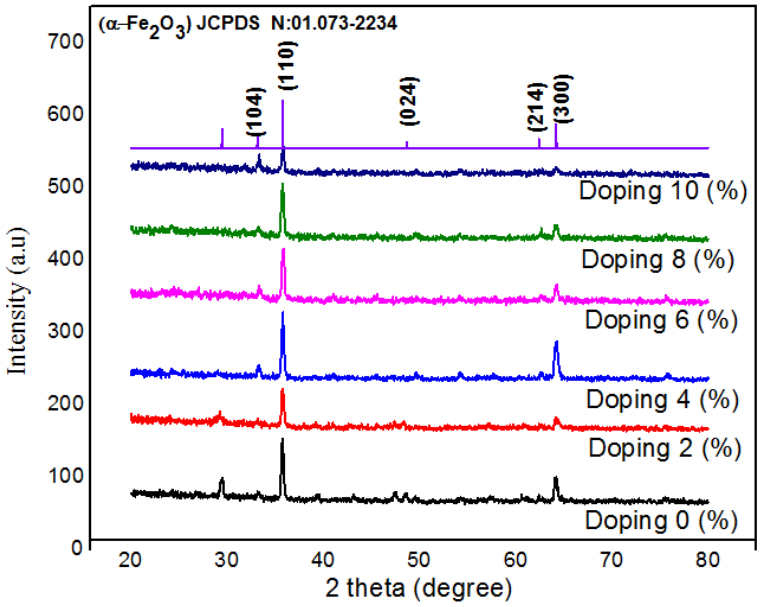

Fig 3. Diffractogramme des rayons X de la poudre de α-Fe_2O_3

The XRD patterns of as-deposited and annealed thin films are presented in Figure 3. The observed peaks at 2θ: 33.54°,37.78°, 49.73°, 62.50°, and 64.47°correspond to lattice planes of (104), (110),(024), (214), and (300), respectively. This finding supports the idea that expanded films have a rhombohedral crystal structure and agrees with the Joint Committee of thin films Diffraction System (as mentioned in reference) (JCPDS No: 01.073- 2234, with space group R-3c number 167). As shown in figure 3, for doped samples, all the observed peaks in the case of non doped samples persevere with approximately fixed slight shift to lower 2θ values for all Aluminum doping concentration. This shift may be due to bigger radius of Aluminum, compared to iron one (R(Fe)=126pm=126*10^-12 m R(AL)=143pm=143*10^-12 m) [5].

On other hand, comparison between different diffractograms of pure and doped α-Fe2O3 shows shift in diffraction angle position of (110) peak towards large values for all doping rates, as shown in figure3. This leads to the conclusion that α-Fe_2O_3 lattice in elaborated layers is in compression state. The difference is usually reported in previous works and could be due to doping atoms incorporation in substitutional or interstitial positions [22, 23]. We can also see that small size of aluminum (R Al^{3+} = 0.05 nm) compared to that of iron (R Fe^{3+} = 0.064 nm), meshes compression cause.

Except that (110) peak reached greatest value for 4% doping; after having undergone a decrease for 2%, it continues to stabilize thereafter until a total decrease to 10%; same pace of element (110), followed by others peaks (300). (214). (104).

The appearance of element 104 from 4% doping; continues to have a progressive pace up to 10% doping. (Figure 4)

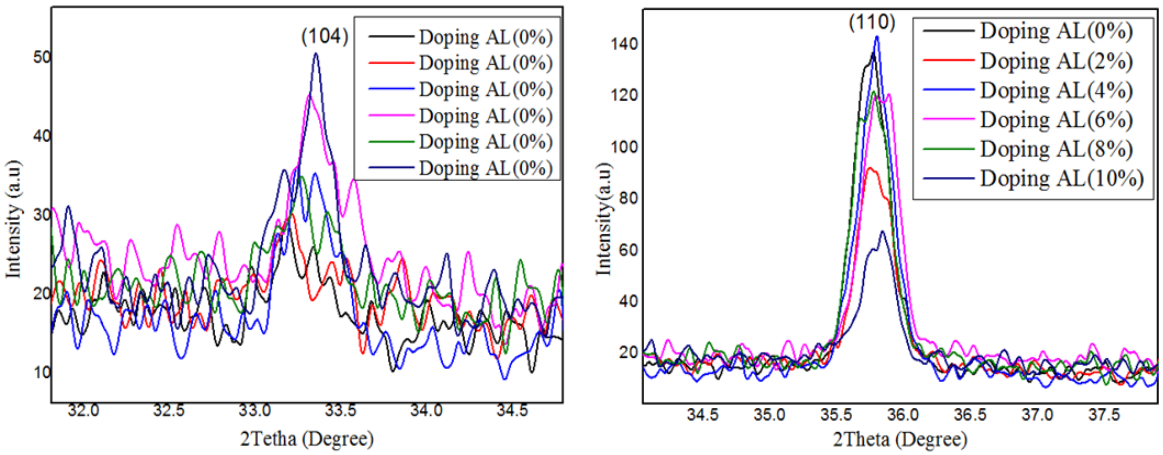

Fig. 4. Variation of the angular position of (110) and (104) peak as a function of doping rate.

3.1.2. Crystallite size calculation

Crystallite size for the (110) plane of thin films of pure and doped α-Fe_2O_3aluminum was estimated using X-ray diffraction using the Debye-Scherrer. Calculations obtained are recorded in table 1 and represented in figure 4. We see that the sizes found are small in nanometers order, varying between 13.51 and 16.12 nm for all thin films of pure and doped α-Fe_2O_3.

Decrease in crystallites size for a few doping percentages such as 6%, may have a relationship with disorder created inside lattice, due to substitution of Fe^{3+} ion by another Al^{3+} ion of different size. There is therefore a structural degradation of deposited films. While increase in crystallites size may be due to incorporation of doping atoms in interstitial sites.

Different texture coefficient TC(hkl) have been derived from the X-ray data to get more information about the favored growth paths. The relative degree of preferred orientation among crystal planes is measured by TC(hkl), which is stated using the formula below[19]:

$$TC(hkl) = \frac{I(hkl)/I_0(hkl)}{N^{-1}\sum_n^N I(hkl)/I_0(hkl)} \quad (1)$$

where I(hkl) is the measured relative intensity of a plane (hkl), I_0(hkl) is the JCPDS-derived standard intensity of the plane (hkl), N is the reflection number, and n is the number of diffraction peaks. Figure 3 shows a maximum TC value along the (110) direction with no difference in TC(hkl) values at different doping percentages.

The lattice constants (a and c), for the rhombohedral phase structure, are determined by the relations [24]

$$2d_{hkl}\sin(\theta) = n\lambda \quad (2)$$

and

$$\frac{1}{{d_{hkl}}^2} = \frac{4}{3a^2}(h^2 + k^2 + hk) + \frac{l^2}{c^2} \quad (3)$$

Table 1. 0-10wt.% Al doped thin films parameters: dhkl,, average grain size, lattice parameters, optical gap.

Doping (Al)%	hkl	2θ (°)	Lattice parameters (Å)	Calculated d(Å)	Average grain size (nm)	Eg (eV)
0%	104	33.16	a=5.02 c=13.77	2.7	15.25	2.59
	110	35.78		2.51		
	024	48.68		1.87		
	214	62.42		1.49		
	300	64.19		1.45		
2%	104	33.23	a=5.02 c=13.73	2.7	15.43	2.64
	110	35.75		2.51		
	024	48.38		1.85		
	214	62.42		1.49		
	300	64.18		1.45		
4%	104	33.26	a=5.02 c=13.72	2.7	16.12	2.74
	110	35.81		2.50		
	024	49.67		1.83		
	214	62.6		1.48		
	300	64.19		1.45		
6%	104	33.32	a=5.01 c=13.7	2.69	15.85	2.597
	110	35.9		2.5		
	024	49.64		1.84		
	214	62.72		1.48		
	300	64.22		1.45		
8%	104	33.26	a=5.02 c=13.71	2.7	13.51	2.781
	110	35.78		2.51		
	024	49.58		1.84		
	214	62.66		1.48		
	300	64.66		1.45		
10%	104	33.35	a=5.02 c=13.66	2.69	13.54	2.64
	110	35.84		2.50		
	024	49.7		1.83		
	214	62.78		1.48		
	300	4.19		1.45		

The inter-planer distance and Miller indices, respectively, are 'd_{hkl}' and (hkl). Table1 shows the values of the lattice parameters 'a' and 'c.' It's worth noticing that the pure sample values (a = b =5.022, c = 13.717) are close to the ones of the standard JCPDS data card, (a_0 =b_0 = 5.0325Å and c_0 = 13.7404Å)[2].

XRD measurement as function of dopant concentration, the increase in lattice parameter of Al-doped hematite thin films compared with no doped one is due to substitution of larger ionic radii of C^{2+} into position of smaller ionic radii of Fe^{3+} in α-Fe_2O_3 lattice. Those values are increased by very small amount up to 2wt.%, this confirms elongation of unit cell along c-direction hence Δc more than Δa. The constant values of lattice parameter after 2wt.% of Aluminum doping may refer to that the substitution process of iron ions has been saturated. The crystalline sizes of thin films in different doping concentration given in table1 were calculated for more appeared peaks then make the average values by using Scherrer's formula[22].

$$D = \frac{0.9\,\lambda}{\beta cos\theta} \tag{4}$$

where D, β, λ, and θare, respectively, the crystallite size, full width at half-maximum (FWHM) of the investigated diffraction peak, X-ray wavelength (1.5406 Å), and Bragg angle[9][19].

Table 2. Grain size and optical gap's variation.

Doping %	0%	2%	4%	6%	8%	10%
Lattice parameters (Å)	a=5.02 c=13.77	a=5.02 c=13.73	a=5.02 c=13.72	a=5.01 c=13.69	a=5.02 c=13.7	a=5.02 c=13.66
Average grain size(nm)	15.25	15.43	16.12	15.85	13.51	13.54
Eg (eV)	2.6	2.64	2.74	2.6	2.8	2.64

Shown in Table2, is the Crystallite size variation; it increases from 15.25 nm for undoped hematite nanoparticles to 15.43 nm for 2% doping. By increasing the doping concentration to 4%, crystallite size increases to 16.12nm. For doping concentration of 6%, crystallite size is reduced to 15.85nm; this value keeps decreasing to 13.51nm for 8% and 13.54 till 10% doping concentration. Decrease in crystallite size at doping concentration starting from 8%, can be attributed to presence of Aluminum ions which coincide with oxygen forming its own oxide AlO , this can be defined as crystal defects which well match with increasing in the urbache energy. The reduction in crystallite size was observed as a result of Aluminum oxide presence in the films.

3.1.3. Crystallite size and optical gap's variation

Crystallite size and optical gap's variation, as function of doping rate, are illustrated in figure5. Behavior of confinement quantum which stipulates that size reduction causes the gap increase appears clearly until 10% doping level gives correlation rise between optical gap and crystallites size where they vary in a similar way; when crystallites size increases, optical gap also increases.[22-23].

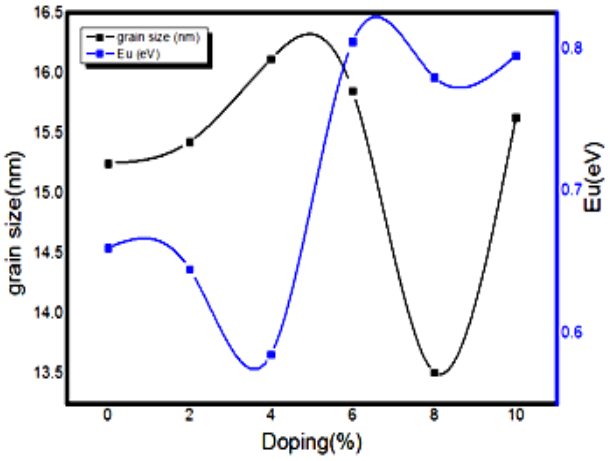

Fig 5. Variation in grain size and optical gap as a function of doping rate.

3.2.Thin film optical characterization of pure and Al-doped α-Fe_2O_3

To complete our analyses, we correlated structural measurements with optical measurements.

3.2.1. Optical transmittance

Transmittance spectra of pure and aluminum-doped α-Fe_2O_3 thin films are shown in figure 6. The general shape of spectra is identical; they are composed of two regions:

Region of strong absorption, that corresponds to fundamental absorption ($\lambda < 600\ nm$) in α-Fe_2O_3 films. Transmittance begins to cancel out below about 600 nm. This cut-off corresponds to optical gap (band gap) of α-Fe_2O_3; all photons with energy above the gap are absorbed instead of being transmitted [9]. Variation transmittance, this region is exploited for gap determination. It's observed that transmittance band is formed by several gaps, which are attributed to direct and indirect transitions in the α-Fe_2O_3 semiconductor. Moreover, we see the shift of transmittance band towards the small wavelengths and it begins to move towards long wavelengths for 4% of doping, then towards small wavelengths from 6 %. Region of high transparency located between 550 and 800 nm, varies between 40 and 98%[25]. These values give the thin layers of α-Fe_2O_3 the character of transparency in the visible. The high transparency is one of properties, that explains, thin films of α-Fe_2O_3 interest.

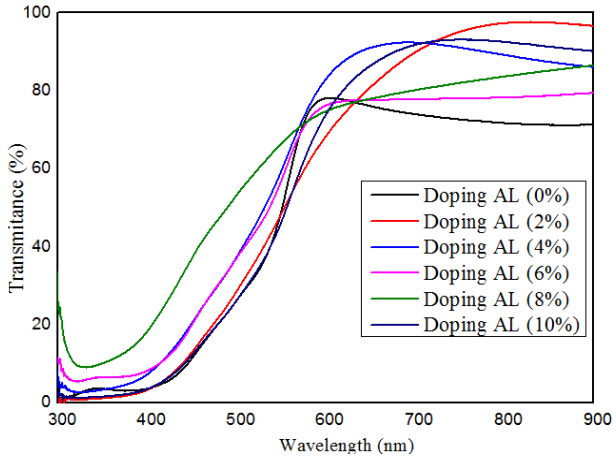

Fig. 6. Thin films transmittance spectra of pure and Al-doped α-Fe_2O_3 for different doping rates.

3.2.2. Gaps optical calculation

Optical gap (the forbidden band) Eg of thin layers pure and Al-doped α-Fe_2O_3 was determined from the transmittance spectra. Exploitation of transmittance spectra according to derivative method, by using the software origin, leads to gap's energy determination. curves show strong band located around 0.8 eV (Figure 6). This value is due to the directed transition of α-Fe_2O_3 semiconductor which is attributed to optical gap Eg of α-Fe_2O_3 [19].

Table 3. Thin films optical gap of pure and Al-doped α-Fe_2O_3.

Annealing time	Doping (%)	Optical gap E_g(eV)	Urbach energy E_u(eV)
1h	0	2. 59	0.66
	2	2.63	0.65
	4	2.74	0.59
	6	2.6	0.81
	8	2.77	0.78
	10	2.59	0.8

The effect of aluminum atoms incorporation on the gap of α-Fe_2O_3 is apparent from which we notice a shift in the forbidden band in the presence of aluminum (Table 3 and Figure 7). In addition, gap increased from 2.59 for pure, reaching 2.74 eV for 4% doping, then it decreases by 6% and it grows to reach the maximum value of 2.78 for 8% doping and decreases again reaching the value of 2.59. Thus, we also see the appearance of weak bands located at 2.63 and 2.60 eV; which are assigned to indirect transitions within the energy levels [8].

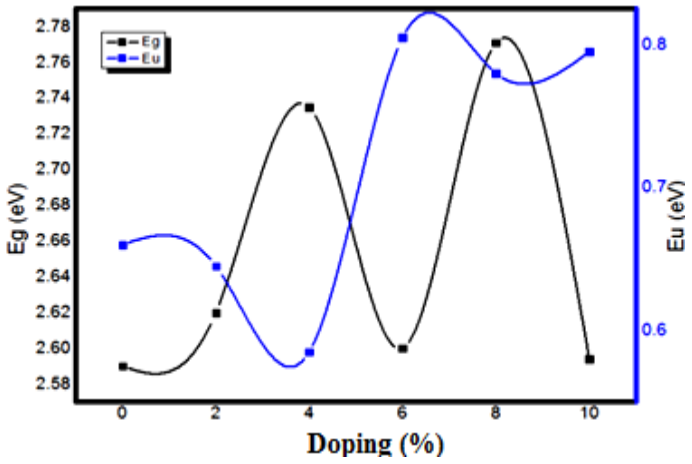

Fig. 7. Variation in h ν function of doping %.

The increase in thin layers gap of aluminum doped α-Fe_2O_3 is mainly due to the effect of Burstein and Moss [24] which increases the optical gap with the increase in the concentration of charge carriers(electrons). This caused filling of conduction band states by electrons coming from doper due to low density of semiconductor states of minimum near band conduction.

3.3. Optical properties

Photos of elaborated thin films are presented in Figure 6 which exhibits the change in color as a function of doping concentration. Figure 7 shows the transmittance spectrum of 0-10wt% Al-doped thin films. For undoped sample, the transmittance spectrum was found to be about 76% beyond 550nm. For the doped ones, this value decreases to reach 65% at doping concentration 8%, then increases to exceed 98% for 2%, 4 and 10% wt Al-doped samples whereas for 88 % Al-doped sample the value of transmittance becomes lower than 75%. Bellow 550 nm, the transmittance spectrum displays a drastic decrease due to the fundamental absorption of the materials (*i.e* the band gap).

The band gap has been calculated using, Tauc's relation as follow [26]:

$$\alpha h\nu = A(h\nu - Eg)^n \quad (5)$$

A is a constant and n is taken 2 based on the fact that α-Fe_2O_3 has an indirect gap. [26, 19]. The optical absorption data was used to plot $(\alpha h\nu)^2$ vs hν, as shown in Fig.8, the straight line extrapolation leads to the band gap energy values of 0-10 wt % Al-doped samples.

An obvious increase (blue shift) in *Eg* for the Al-doped hematite thin films compared to the non doped ones; *Eg* increases from 2.59 for pure α-Fe2O3 to 2.63, 2.74, 2.6, 2.77and 2.59eV in respect to the doper concentration 2%, 4%, 6%, 8%, and 10 wt.%, respectively. It is worth noting that the first ionization energy of Al (5.98eV) is less than that of one of iron (7.90eV) leading to a localization 3d orbital of Aluminum higher than the 3d orbital of iron This can cause active transitions engaging 3d levels in Al^{+2} ions and strong pd-d exchange interaction between itinerant pd α-Fe_2O_3 orbits and the restricted d of the doper. As a result a narrowing in the conduction band *EC* and the valence band *EV* happens and causes a shift of *EC* upwards and *EV*

downwards, which leads to proclaim that Al doping causes the band gap to broaden. The same phenomena (blue shift) are carried out in the literatures [[22],[23], [27][28]].

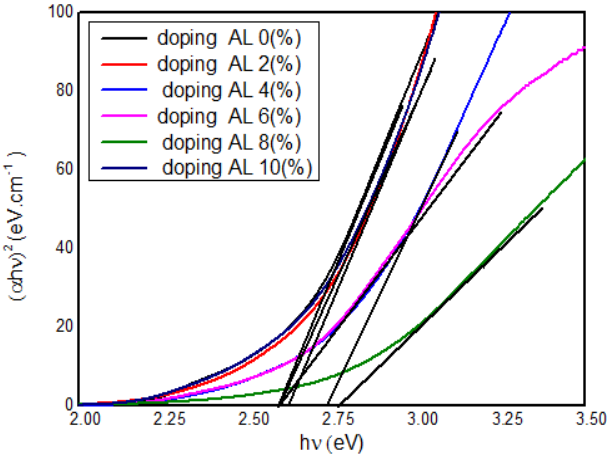

Fig 8. The estimated band gap (E_g) from Tauc's relation for 0-10%wt Al-doped α-Fe_2O_3 thin films.

hν(eV), are in the same value for the cases of 0, 6 and 10 % doping, however, 2% has a little difference. 4% and 8 % doping aluminum in oxid iron, give us more value of hν with little difference.

3.4. FTIR analysis

FTIR analysis was used to characterize the Al–OH vibrations, as shown in figure 9, at vibrational frequencies of 1645 cm1. This investigation also discovered that absorbance rose at frequencies of 500 cm1,796 and 1000 cm1, which is connected to doping percentage with a high value of 8%, of Fe-O and Al-O, implying a phase change into the state -Fe2O3 in the 4% dopant. The band gap dropped with an increase in the Al dopant in the UV-DRS investigation, from 2.59 eV for a pure -Fe2O3 to 2.74 eV for a sample with a 4% dopant, which is less than the band gap energy of 6–8 eV obtained by several researchers.[29] [27].

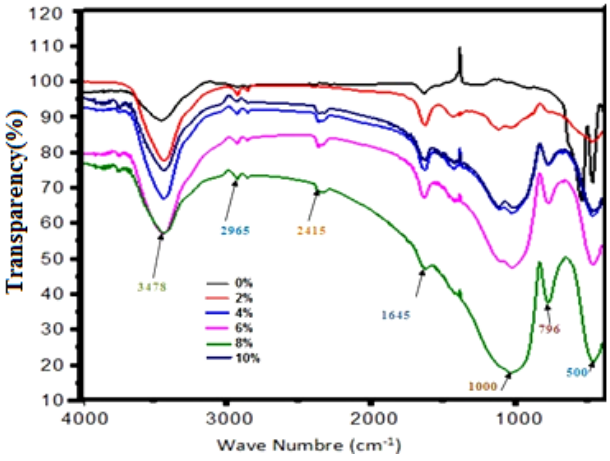

Fig. 9 . FTIR spectrum of α-Fe_2O_3 of pure and Al-doped thin films.

FTIR results also revealed that absorption peak at a wave number of 3478 cm^{-1} is related to activation of OH radicals[30]. at 6 and 8 doping percentage. The incorporation of aluminum

atoms in the Fe_2O_3 lattice was confirmed. However, the analysis shows that only some aluminum atoms were incorporated [31]. Peaks of 2415 and 2965 cm^{-1} confirm the presence of C-C and C-H .

4. Conclusion

The main results obtained during this study confirm the presence of diffraction peaks corresponding to planes (104), (110), (024), (214), and (300) signified hematite phase formation. As a result of doping, one added peaks appeared much well to planes which correspond to Aluminum oxides AlO. The peaks positions corresponding to hematite marked a fixed slight shift to lower 2θ values for all Aluminum doping concentrations. The X-ray diffraction results confirmed the formation of the α-Fe_2O_3 semiconductor of corundum-like trigonal structure with preferential orientation following the plane (110) and a displacement of the diffraction peaks towards large angles when the doping rate increases. X-ray diffractograms also help us to calculate crystallite size.

The optical characterization from the spectra of transmittance in the spectral range 550-800 nm showed that the pure and doped layers are transparent with a value of the order of 40 to 98%. We also obtained a displacement of the optical gap towards high energies for the 2% dopings then towards low energies for 8% followed by an increase from 4% doping, indicating the widening and then the reduction of the forbidden band.

Crystallite size increases in doping beginning then it takes a successive reduce values in increase doping concentration. Optical transmittance and band gap values increase with increasing doping concentration. FTIR study confirms the existence of both Iron and Aluminum oxides. The results of the FTIR revealed that the absorption peak at the wave number of 3455 cm1 is related to the activation of OH radicals. With an elevation of dopant at 6% and 8%.

It can be deduced that 2% doping is best doping which makes it possible to obtain a high transmittance and 4% has high electron energy.

Acknowledgments

This work was supported in part by the VTRS Laboratory, College of Technology, University of. Measurement of UV-visible data The X-ray diffraction data in this work was obtained using an XPERT-PRO diffractometer and are Supported by a Physico-chemical laboratory for mineral materials and their applications at the University of M'Sila

References

[1] Alaa A. Akl, Applied Surface Science 221, 319 (2004); https://doi.org/10.1016/S0169-4332(03)00951-6

[2] Abhijit A. Yadav, T.B. Deshmukh, R.V. Deshmukh, D.D. Patil, U.J. Chavan. Thin Solid Films, (2016); https://doi.org/10.1016/j.tsf.2016.08.062

[3]Ali Badawi, Applied Physics A 128:123 (2022); https://doi.org/10.1007/s00339-021-05154-9

[4] Beril K. Ozcelik , Celaletdin Ergun, Ceramics International411994-2005(2015); https://doi.org/10.1016/j.ceramint.2014.09.103

[5] S. O. Lee, T. Tran, B. H. Jung, S. J. Kim, and M. J. Kim, Hydrometallurgy 87 9199 (2007); https://doi.org/10.1016/j.hydromet.2007.02.005

[6] M. Benamara, N. Zahmouli, S. Soreto Teixeira, M. P. F. Graça, L. El Mir, M. A. Valente, Journal of Electronic Materials, (2022); https://doi.org/10.1007/s11664-022-09539-1

[7] R. Chiarizia and E. P. Horwitz, New formulations for iron oxides dissolution, 27 339-360 (1991); https://doi.org/10.1016/0304-386X(91)90058-T

[8] Bruno Mauvernay, Thèse de Doctorat, Université de Toulouse III (2007).

[9]D.Bekkar, Y.Meftah, B.Benhaoua, A.Rahal, A.Benhaoua,A..H.Hamzaoui, Journal of Optoelectronic and Biomedical Materials. 33 - 42 (2020).

[10] Richard B. Frankel, Iron oxides, from nature to applications, Ed. Damien Faivre (2016).

[11] G. Zelmanov, R. Semiat, Water research 42(1) 492 (2008); https://doi.org/10.1016/j.watres.2007.07.045

[12] S. He, Y. Feng, J. Ni, Y. Sun, L. Xue, Y. Feng, Y. Yu, X. Lin, L. Yang, Chemosphere 147, 195 -202 (2016); https://doi.org/10.1016/j.chemosphere.2015.12.055

[13] H. J. Shipley, K. E. Engates, A. M. Guettner, Journal of Nanoparticle Research 13 (6), 2387 - 2397 (2011); https://doi.org/10.1007/s11051-010-9999-x

[14] Y. Cheng, X. Zhao, X. Liu, W. Sun, H. Ren, B. Gao, J. Wu,International Journal of Nanomedicine 10, 727 (2015); https://doi.org/10.2147/IJN.S75706

[15] A. Ubale, M. Belkhedkar, Journal of Materials Science & Technology 31(1), 1 (2015); https://doi.org/10.1016/j.jmst.2014.11.011

[16] D. K. Kim, M. Mikhaylova, Y. Zhang, M. Muhammed, Chemistry of Materials 15(8), 1617 (2003); https://doi.org/10.1021/cm021349j

[17] S. Schwarz, J. E. Wong, J. Bornemann, M. Hodenius, U. Himmelreich, W. Richtering, M. Hoehn, M. Zenke, T. Hieronymus, Nanomedicine: Nanotechnology, Biology and Medicine 8(5), 682 (2012); https://doi.org/10.1016/j.nano.2011.08.010

[18]Mohammad Shahnawaze Ansari, Mohd Hafiz Dzarfan Othman, Mohammad Omaish Ansari,Sana Ansari, Huda Abdullah, Applied Materials Today, 2021

[19] Y. Meftah, D. Bekker, B. Benhaoua, A. Rahal, A. Benhaoua, A. Hamzaoui, Digest Journal of Nanomaterials and Biostructures, 13(2), 465 (2018).

[20] Aseya Akbar, Hassan Yousaf, Saira Riaz, Shahzad Naseem, Journal of Magnetism and Magnetic Materials, (2019); https://doi.org/10.1016/j.jmmm.2018.09.008

[21] Ferretto L, Glisenti A., J Mol Catal A: Chem, 187: 119(2002); https://doi.org/10.1016/S1381-1169(02)00126-7

[22] F.F.H. Aragón, J.D. Ardisson, J.C.R. Aquino, I. Gonzalez, W.A.A. Macedo, J.A.H. Coaquira , J. Mantilla, S.W. da Silva, P.C. Morais, Thin Solid Films 607, 50. (2016); https://doi.org/10.1016/j.tsf.2016.03.052

[23] M. Lie, H. Fjellvåg, A. Kjekshus, Thin Solid Films 488 74-81 (2005); https://doi.org/10.1016/j.tsf.2005.04.063

[24] Fu H, Quan X, Zhao H. Photodegradation of -HCH by _-Fe2O3and the influence of fulvic acid. J Photochem Photobiol Chem,2005, 173: 143 https://doi.org/10.1016/j.jphotochem.2005.01.013

[25]Aimane Guedri, Mourad Zaabat, Boubekeur Boudine, Abdelkader Hafdallah, " Research Square Platform LLC, (2021); https://doi.org/10.21203/rs.3.rs-821148/v1

[26] Liu Y, Sun D., J Hazard Mater, 143: 448(2007); https://doi.org/10.1016/j.jhazmat.2006.09.043

[27] Wu, X.J., Zhang, Z.Z., Liang, Q.S. and Meng, J., J. Cyrs. Growth, 340, 74-77. (2012); https://doi.org/10.1016/j.jcrysgro.2011.12.041

[28] Said Benramache, Boubaker Benhaoua, Superlattices and Microstructures, (2012); https://doi.org/10.1016/j.spmi.2012.06.005

[29] Abolfazl Khodadadi, Majid Farahmandjou, Mojtaba Yaghobi, Materials Research Express, (2018); https://doi.org/10.1088/2053-1591/aaef70

[30] Azam Jafari, Siamak Khademi, Majid Farahmandjou, Ahmad Darudi, Reza Rasuli, Journal of Electronic Materials, (2018); https://doi.org/10.1007/s11664-018-6590-1

[31] Yanagihara, H., Myoka, M., Isaka, D., Niizeki, T., Mibu, K. and Kita, E., J.Phys. D: Appl. Phys., 46, 17500. (2013); https://doi.org/10.1088/0022-3727/46/17/175004